

1 **Unraveling the causal genes and transcriptomic determinants of** 2 **human telomere length**

3 Ying Chang^{1, #}, Yao Zhou^{2, #}, Junrui Zhou^{3,4, #}, Wen Li¹, Jiasong Cao¹, Yongmei Shen¹,
4 Xutong Fan², Hongxi Yang^{2,5}, Xiaobao Dong³, Shijie Zhang⁵, Xianfu Yi², Ling Shuai⁶,
5 Lei Shi⁷, Zhe Liu⁷, Jie Yang⁷, Jihui Hao⁸, Kexin Chen⁹, Dandan Huang^{5,*}, Feng Wang^{3,*},
6 Mulin Jun Li^{2,9,*}

7 ¹Tianjin Key Lab of Human Development and Reproductive Regulation, Tianjin Central
8 Hospital of Obstetrics and Gynecology, Nankai University, Tianjin, China.

9 ²Department of Bioinformatics, The Province and Ministry Co-sponsored Collaborative
10 Innovation Center for Medical Epigenetics, Key Laboratory of Immune Microenvironment and
11 Disease (Ministry of Education), School of Basic Medical Sciences, Tianjin Medical
12 University, Tianjin, China.

13 ³Department of Genetics, School of Basic Medical Sciences, Tianjin Medical University,
14 Tianjin, China.

15 ⁴Department of Clinical Laboratory, Shanghai Children's Hospital, Shanghai Jiaotong
16 University, Shanghai, China.

17 ⁵Department of Pharmacology, Tianjin Key Laboratory of Inflammation Biology, School of
18 Basic Medical Sciences, Tianjin Medical University, Tianjin, China.

19 ⁶State Key Laboratory of Medicinal Chemical Biology, College of Pharmacy, Tianjin Central
20 Hospital of Gynecology Obstetrics/Tianjin Key Laboratory of Human Development and
21 Reproductive Regulation, Nankai University, Tianjin, China.

22 ⁷Key Laboratory of Immune Microenvironment and Disease (Ministry of Education), School of
23 Basic Medical Sciences, Tianjin Medical University, Tianjin, China.

24 ⁸Department of Pancreatic Cancer, Key Laboratory of Cancer Prevention and Therapy,
25 National Clinical Research Center for Cancer, Tianjin Medical University Cancer Institute and
26 Hospital, Tianjin, China.

27 ⁹Department of Epidemiology and Biostatistics, Tianjin Key Laboratory of Molecular Cancer
28 Epidemiology, National Clinical Research Center for Cancer, Tianjin Medical University
29 Cancer Institute and Hospital, Tianjin Medical University, Tianjin, China.

30
31 #The authors contributed equally to this work

32 *Correspondence: mikey.huang2011@gmail.com (D.H.), wangf@tmu.edu.cn (F.W.),
33 mulinli@connect.hku.hk (M.J.L.)

34

35 **Abstract**

36 Telomere length (TL) shortening is a pivotal indicator of biological aging and is associated with
37 many human diseases. The genetic determinants of human TL have been widely investigated,
38 however, most existing studies were conducted based on adult tissues which are heavily

39 influenced by lifetime exposure. Based on the analyses of terminal restriction fragment (TRF)
40 length of telomere, individual genotypes, and gene expressions on 166 healthy placental tissues,
41 we systematically interrogated TL-modulated genes and their potential functions. We found
42 that placental TL is relatively longer across human tissues and which maintenance is mostly
43 connected to genes responsible for alternative lengthening of telomeres. Trans-ancestral TL
44 genome-wide association studies (GWASs) on 644,553 individuals identified 20 novel genetic
45 associations and provided increased polygenic determination of human TL. Next, we integrated
46 the powerful TL GWAS with placental expression quantitative trait locus (eQTL) mapping to
47 prioritize 31 likely causal genes, among which 4 were functionally validated, including *MMUT*,
48 *RRM1*, *KIAA1429*, and *YWHAZ*. Finally, modeling transcriptomic signatures and TRF-based
49 TL improved the prediction performance of human TL. This study deepened our understanding
50 of causal genes and transcriptomic determinants of human TL, promoting the mechanistic
51 research on fine-grained TL regulation.

52

53 **Introduction**

54 Telomeres are DNA and protein complexes that protect the ends of chromosomes, yet
55 degradative processes that shorten telomeric DNA can lead to loss of telomere function and
56 genomic instability ^{1,2}. Telomeres shorten with each round of DNA replication in the
57 organism's aging process ³. Thus, telomere length (TL) has been recognized as a critical
58 indicator of cellular senescence, biological aging, and disease progression ⁴⁻⁶. In previous
59 studies, determinants of human TL have been extensively interrogated, including different
60 genetic, environmental, and lifestyle factors ^{2,7}. For example, genetic variants associated with
61 TL have been systematically identified through family studies ^{8,9} and genome-wide association
62 studies (GWASs) ¹⁰⁻¹². Non-genetic factors, such as cigarette smoking ¹³, alcohol consumption
63 ¹⁴, and endurance training ¹⁵, could modulate telomere attrition processes. In addition, a
64 large-scale cross-tissue TL analysis revealed that TL varied across tissue types and was the
65 shortest in whole blood ¹⁶. Despite these successes, most of the current studies on human TL
66 were performed on postnatal or adult tissues, which confounds the understanding of
67 independent determinants from genetic or environmental factors, especially for
68 non-Medawarian tissues affected by unobserved lifetime exposures ^{17,18}.

69 Current TL GWASs have uncovered more than a hundred genomic loci significantly associated
70 with leukocyte TL ¹⁰⁻¹², however, the true causal genes underlying these polygenic
71 determinants of TL remain elusive. The majority of the identified associations lie in the
72 non-coding regions of the human genome, suggesting that causal variants could influence TL
73 via gene regulatory codes. Expression quantitative trait loci (eQTLs) analysis using gene
74 expression as a key intermediate molecular phenotype, improves the functional interpretation
75 of GWAS findings ¹⁹. Thus, integrating powerful TL GWAS results with eQTLs on tissue
76 rarely affected by non-genetic factors would enhance the TL-causal gene discovery ^{20,21} and

77 also facilitate accurate TL prediction by incorporating both genomic and transcriptomic
78 information.

79 In the present study, by assuming that telomere is less affected by extraplacental exposure or
80 other non-genetic effects in the placenta, we profiled terminal restriction fragment (TRF) length
81 of telomere, genotypes, and gene expression on 166 healthy placental tissues. We found that
82 placental TL expresses the intra-tissue homogeneity and is longer across human tissues, except
83 for testis. The analysis of gene expression association with placental TL revealed several
84 unique telomere-maintaining patterns. Importantly, we integrated three large-scale TL
85 GWASs from worldwide cohorts and performed a trans-ancestral meta-analysis. Then,
86 placental eQTL mapping and complementary statistical approaches were leveraged to
87 comprehensively prioritize the putative causal genes affecting TL phenotype. We also
88 experimentally validated several novel TL-causal genes *in vitro*. Finally, we developed an
89 accurate TL prediction model that outperforms the existing strategies.

90

91 **Results**

92 **TL in the placenta expresses intra-tissue homogeneity and is longer across tissues**

93 To measure the telomere-associated phenotypes of human tissues at the early life stage, we
94 conducted population-scale southern blots of TRFs²², an accurate characterization of telomeres,
95 on 166 healthy placental tissues (see methods for details). These placentae were collected
96 within 10 min of a vaginal delivery from full-term singleton pregnancies (37⁺⁰–41⁺⁶ weeks)
97 (Fig. 1A), and none of the participants had any medical disorders or adverse pregnancy
98 outcomes. The average age of the participants was 32 ± 4.0 years, and no tobacco-smoking or
99 alcohol-drinking behavior was noted. Among these newborns, 73 were females and 93 were
100 males. No significant differences were observed in maternal age, maternal body mass index
101 (BMI), infant weight, and gestation weeks with regard to infant gender (all *P*-values > 0.05)
102 (Supplementary Table 1). In addition to these placental tissues, genotypes [the Infinium Asian
103 Screening Array (ASA), *n* = 166] and gene expression (RNA-seq, *n* = 166) were also profiled
104 for in-depth analysis of the causal genes and transcriptional determinants of placental TL (Fig.
105 1B).

106 Previous studies reported that the TRF length of telomere is highly synchronized among
107 various tissues at birth, whereas in adults, TL across tissue types varies within individuals^{16,23,24}.
108 The sampling of eight symmetrical sets of placental tissue on the fetal side and maternal side
109 revealed a consistent distribution of telomere fragments, suggesting a homogeneous telomere
110 status across the whole placenta (Fig. 1C). However, compared to intraplacental telomere status,
111 the ranges and variances in TRF lengths were enlarged as assessed by randomly sampling of 15
112 unrelated individuals (Supplementary Fig. 1). These results implied that the telomere content of

113 placental tissue varies among individuals and could be attributed to varied genetic conditions
114 and intrauterine environments.

115 Since the southern blot of TRF contains abundant information on telomere content, based on
116 TRF analysis of the fetal side placental tissues from 166 unrelated singleton pregnancies, we
117 quantified the average TRF length (aTL), relative TL (RTL), and short telomere proportion
118 (STP), respectively (see methods for details). Briefly, the RTL was used to evaluate the aTL
119 relative to a standard reference, and the STP measured the percentage of the telomere shorter
120 than 5 kb over fragments, indicating severe telomere damage or wear ²⁵. Placental aTL ranges
121 from 8.4–17.8 kb among 166 placental tissues (mean = 11.9 kb). Leveraging GTEx RTL data of
122 48 different adult tissues revealed that RTL in the placenta is longer than that of most of other
123 tissues, except the testis (Fig. 1D). This conforms to the expectation that TL is associated with
124 cellular senescence; it is maximal at birth and decreases with age and exposure ²⁶. No clear
125 association was observed between RTL and the collected demographic factors, including
126 maternal age, gestational days, maternal BMI, infant weight, and placental size (Supplementary
127 Fig. 2). Notably, neonatal sex showed weak evidence of association with RTL in the placenta,
128 wherein males have longer RTL than females (*P*-value = 0.032, *t*-test, Supplementary Fig. 2).
129 Given the limited sample size of our existing TRF measurements in newborns ^{23,27}, the
130 underpowered associations require further ascertainment on large-scale samples. Moreover, the
131 current data revealed that placental STP was negatively correlated with RTL (Fig. 1E),
132 indicating the dependency between TL and short telomere, and RTL could partially explain
133 telomere damage. However, we did not observe significant differences between placental STP
134 and any collected demographic factors (Supplementary Fig. 3). Taken together, the intra-tissue
135 homogeneity of telomere content, long RTL across tissues, as well as less external
136 environmental intervention make placental tissue an ideal proxy for studying the genetic
137 determinants and causal genes of human TL.

138

139 **Trans-ancestral GWAS reveals increased polygenic determination of TL**

140 In order to explore the extent of genetic contribution on TL, we first integrated several
141 large-scale TL GWASs from different cohorts on worldwide populations, including Singapore
142 Chinese Health Study (SCHS) ¹⁰, NHLBI Trans Omics for Precision Medicine (TOPMed) ¹²,
143 and UK Biobank (UKBB) ¹¹. Next, we conducted a trans-ethnic meta-analysis based on these
144 leukocyte TL GWASs, containing 644,553 participants from five human subpopulations
145 (including European, African, East Asian, South Asian, and Hispanic/Latino) (Fig. 2A, 2B and
146 Supplementary Table 2) (see methods for details). A total of 222 sentinel variants (>10 Mb
147 between sentinels) were associated with leukocyte TL at genome-wide statistical significance
148 threshold (*P*-value < 5E-8), of which 20 variants were new ($R^2 < 0.01$ with previously
149 documented sentinels) (Supplementary Table 3 and Supplementary Table 4). The
150 meta-analysis revealed 87% (175) of the 201 previously reported TL GWAS significant loci,
151 whereas the remaining 13% (26) loci displayed potential heterogeneity among the three

152 investigated cohorts. Among the newly discovered loci, the most significant sentinel variant
153 rs10798002 received moderate signals in UKBB and TOPMed cohorts and reached
154 genome-wide significance after meta-analysis, but there was no evidence of the effect of
155 heterogeneity across cohorts ($P_{het} = 0.899$, $I^2 = 0$) (Fig. 2C). This variant is located in the
156 *SWI1* gene, affecting the surveillance of nuclear messenger ribonucleoprotein particles ²⁸.
157 Gene-set enrichment analysis of these TL GWAS signals identified that the most significantly
158 associated pathways were related to telomere maintenance, telomere organization, and
159 telomere maintenance via telomere lengthening (Fig. 2D), which is consistent with the
160 previous findings ¹¹ and implies that TL GWAS signals were related to the regulation of
161 telomere maintenance.

162 The trans-ancestral TL GWAS meta-analysis, with the largest sample size to date, provided
163 an effective resource to test the agreement between the genetic determination of TL and
164 observed TL, especially that from fetal tissues under minimal extrauterine intervention. Thus,
165 we genotyped and imputed 6,091,762 genetic variants for the 166 placental samples and
166 performed polygenic risk score (PRS) analyses based on the sentinel significant variants of all
167 independent loci from TL meta-analysis results. The estimated PRS score of TL was
168 significantly correlated with placental TL measured in our study ($r = 0.21$, P -value = 0.007)
169 (Fig. 2E), suppressing the correlations using GWAS summary statistics of the single cohort
170 (Supplementary Fig. 4). This suggested that the trans-ancestral GWAS boosts the predictive
171 power of PRS on TL. Also, no significant differences were observed in the distribution of the
172 individual PRS with respect to sex or maternal age (Supplementary Fig. 5). In contrast, the
173 evaluation of such correlations based on 442 GTEx whole blood samples and 1450 UKBB
174 Chinese leukocyte samples revealed a weak association between TL PRS and tested TL
175 measured by biochemical assays (Fig. 2E). Since GTEx applied a Luminex-based method and
176 UKBB used quantitative polymerase chain reaction (PCR) assay to estimate RTL, these
177 suboptimal measurements may undermine the consistency between PRS-predicted and
178 assayed TL compared to southern blot analysis of TRFs. Collectively, combinatory analysis
179 of trans-ancestral GWAS and placental TL measured by TRF assay indicated that human TL
180 could be determined and predicted only genetically.

181

182 **Placental TL maintenance is associated with alternative lengthening of telomeres 183 (ALT) and functional gene connectivity**

184 Since 91.5% of sentinel variants of TL GWAS loci are located in the non-coding genomic
185 region, investigating their regulatory potential on gene expression would accurately determine
186 TL. Thus, we profiled transcriptomics using RNA-seq for the 166 placental samples with
187 paired genotypes and TL measurements. The expression levels of major telomerase catalytic
188 subunits, including *TERT*, *TERC*, *DKC1*, *NOP10*, *NHP2*, and *WRAP53*, were not correlated
189 with placental RTL (Supplementary Fig. 6), whereas *TERC* and *NHP2* expressions were
190 undetectable in placenta (i.e., transcripts per million (TPM) = 0 in all samples). In addition, a

191 SHELTERIN component *TPP1* showed a moderate correlation with placental RTL ($r = 0.19$,
192 P -value = 0.015) (Fig. 3A), unlike other protein subunits of SHELTERIN and
193 CTC1-STN1-TEN1 (CST) complexes, such as *TINF2*, *RTEL1*, *POT1*, and *CTC1*
194 (Supplementary Fig. 6). Interestingly, we observed that placental RTL was positively
195 correlated with many components of the ATL pathway, including *ATRX* ($r = 0.17$, P -value =
196 0.022), *DAXX* ($r = 0.21$, P -value = 0.008), and *SMARCAL1* ($r = 0.23$, P -value = 0.003) (Fig. 3B
197 and Supplementary Fig. 7), implying that TL maintenance in placenta largely relies on ALT
198 mechanism.

199 Moreover, we found that several canonical telomere maintenance genes were significantly
200 correlated with placental STP, including telomerase catalytic subunits *NOP10* ($r = 0.17$,
201 P -value = 0.026) and *WRAP53* ($r = -0.17$, P -value = 0.025), SHELTERIN component *TPP1* (r
202 = -0.18, p = 0.020), and *RTEL1* ($r = -0.17$, p = 0.031), as well as CST complex member *CTC1* (r
203 = -0.16, p = 0.046) (Fig. 3C and Supplementary Fig. 8). This phenomenon suggested that short
204 telomere phenotype is an effective indicator sensitive to changes in telomere maintenance
205 genes in the placenta. Consistent with the results of placental RTL, placental STP was
206 significantly associated with many genes in the ATL pathway and was negatively correlated
207 with *ATRX* ($r = -0.21$, P -value = 0.006), *SMARCAL1* ($r = -0.22$, P -value = 0.005), *RAD52* ($r =$
208 -0.21, P -value = 0.007), and *POLD3* ($r = -0.22$, P -value = 0.004) (Fig. 3D and Supplementary
209 Fig. 9), further indicating that ALT pathway is dominant in placental telomere attrition and
210 repair.

211 To inspect the underlying biological functions associated with placental TL maintenance, we
212 performed two gene module analyses based on transcriptome data from the 166 placentae. First,
213 we used a weighted gene co-expression network analysis (WGCNA)²⁹ to construct the
214 co-expression networks of the human placenta and identified 26 network modules (Fig. 3E).
215 The correlation test between each module eigengene (ME) score and RTL identified turquoise
216 module was significantly associated with RTL, and the genes in this module were enriched in
217 the ubiquitin-like protein transferase activity (GO:0019787, adjusted P -value = 1.61e-06) (Fig.
218 3E and Supplementary Fig. 10); this finding was supported by previous studies on the
219 ubiquitin-like proteins on telomere regulation^{30,31}. Second, to investigate whether RTL affects
220 gene connectivity in the placenta, we calculated the connectivities of 4679 genes with high
221 variance from the 166 placental RNA-seq data, starting from the upper quarter RTL (left side of
222 Fig. 3F) and subsequently added one sample with shorter RTL and removed one sample with
223 longer RTL to recalculate the connectivities. Based on the hierarchical clustering of the
224 RTL-driven gene connectivities, we detected five gene clusters by Elbow method. For example,
225 1424 genes in cluster 1 were predominantly interconnected among samples with longer RTL
226 and these genes were significantly enriched in the cell adhesion molecule binding
227 (GO:0050839, adjusted P -value = 1.39e-20), while, 585 genes in cluster 4 were highly linked
228 among samples with shorter RTL and these genes were related to receptor ligand activity
229 (GO:0048018, adjusted P -value = 6.16e-09) (Fig. 3G).

231 **Integrating placental eQTL and TL GWAS for systematic prioritization of**
232 **TL-causal genes**

233 Recent genetic studies have identified many novel TL-associated genes by eQTL-based
234 methods^{11,32}, but they mainly employed eQTLs derived from adult tissues, probably leads to
235 biased estimation through unobserved lifetime exposures. A genome-wide *cis*-eQTL mapping
236 on 166 placental samples from Asia population (see methods for details) was conducted to
237 examine novel TL-causal genes based on our trans-ancestral GWAS meta-analysis. Compared
238 to the previous placental eQTLs on European cohort³³, we observed similar distributions of
239 genomic distances to the gene transcription start site (TSS) and end site (TES), but identified
240 3913 more eQTL-associated genes (eGenes) (Supplementary Fig. 11A). The effect sizes of
241 eQTLs in the two cohorts were also correlated (Supplementary Fig. 11B, $r = 0.42$, P -value <
242 2.2E-16). Based on RoadMap chromHMM 15 core states of placenta³⁴, we observed that most
243 of the placental eQTLs are located in the active chromatin regions and significantly enriched in
244 placental active promoter (TssA) and enhancer (Enh and EnhG) states (Supplementary Fig.
245 11C-D). These results indicated the validity and the gained power of our placental eQTL
246 mapping.

247 To systematically prioritize the potential TL-causal genes, we integrated our placental eQTLs
248 and aforementioned trans-ancestral GWAS results using two complementary statistical
249 strategies. First, colocalization analysis via COLOC³⁵ was performed to test the shared causal
250 variants between gene expression (from eQTL) and TL trait (from GWASs). We identified 53
251 signals with strong evidence of colocalization between placental eQTL and TL GWAS loci
252 (posterior probability PP4 ≥ 0.5 , Supplementary Table 5). Second, Fusion
253 Transcriptome-wide association analysis (TWAS)³⁶ and Summary-based Mendelian
254 Randomization (SMR)³⁷ were applied to test for a significant genetic correlation between
255 *cis*-expression and GWAS signal. Thus, we observed 64 genes reaching transcriptome-wide
256 significance (false discovery rate (FDR) ≤ 0.1 , two-tailed Z-test) in TWAS (Fig. 4A,
257 Supplementary Table 6) and identified 61 genes showing a potential association with TL after
258 HEIDI test (FDR < 0.1) in SMR (Supplementary Table 7), respectively.

259 The intersection of gene prioritization results from COLOC and the union of TWAS and SMR
260 retrieved 31 likely causal genes related to TL (Supplementary Table 8). These candidates
261 encompassed several genes responsible for canonical telomere regulation, such as telomere
262 length maintenance³⁸ and telomere end protection³⁹. Moreover, some of the mechanisms
263 underlying the causal genes have been explored recently. For example, *TSPYL5* is required to
264 maintain POT1 protein levels and suppresses POT1 poly-ubiquitination and degradation
265 exclusively in ALT cells⁴⁰. *GEN1* is required for telomere replication and prevents the cutting
266 of telomeres⁴¹. *RFWD3* plays a role in DNA damage response and facilitates translesion DNA
267 synthesis⁴². *ATE1* encodes an arginyltransferase for ubiquitin-dependent degradation and is
268 associated with subtelomeric regulation⁴³. We also discovered several novel genes whose
269 TL-related function was rarely documented, such as *RRM1*, *MMUT*, *KIAA1429*, *YWHAZ*,

270 *PEX6*, *POLI*, *CDC25B*, and *HDDC2*, and exemplified strong evidence of positive causal
271 associations between genetic determined expressions and TL in genomic loci of four novel
272 genes (Fig. 4B–I). Collectively, the stringent prioritization of TL-causal genes based on
273 placental eQTL and large-scale TL GWAS summary information would provide new insight
274 for understanding TL regulation.

275

276 **Experimental validations of top prioritized genes in TL regulation**

277 To evaluate the causal effect of the novel hits in our prioritization, we functionally verified the
278 positive regulation of TL by perturbing the four genes screened above: *RRM1*, *MMUT*,
279 *KIAA1429*, and *YWHAZ*. Briefly, HTR8/SVneo cell lines were established by immortalizing a
280 physiological extravillous trophoblast cell by transfection with a plasmid containing the simian
281 virus 40 large T antigen⁴⁴. Stable HTR8/SVneo cell lines were established by the knockdown
282 of the above four genes by shRNA plasmids. Next, we detected whether TL in these cell lines
283 would shorten via southern blots of TRF assays to verify the likely causal correlation between
284 investigated genes and TL.

285 *RRM1* gene encodes the large and catalytic subunit of ribonucleotide reductase (RNR), an
286 enzyme for converting ribonucleotides into deoxyribonucleotides, which is essential for DNA
287 replication and DNA repair processes⁴⁵. Moreover, it has been established that RNR is crucial
288 for telomere elongation to prevent the early onset of replicative senescence in
289 telomerase-negative cells in budding yeast⁴⁶. In addition, a WGS-based telomere length
290 analysis in Dutch family trios⁴⁷ showed that *RRM1* might also be involved in telomere length
291 regulation in humans. However, the direct correlation between human RNR and TL has not yet
292 been established. Consequently, the knockdown of *RRM1* gene in eight monoclonal
293 HTR8/SVneo lines consistently showed telomere shortening compared to control cells (Fig. 5A
294 and 5B). One cell clone (shRRM1-2-6) was picked for continuous passage. The results
295 demonstrated that TL was gradually shortened with cell passage (Fig. 5C), further confirming
296 the positive regulatory effect of the *RRM1* gene on TL in the placenta.

297 *MMUT* gene encodes the mitochondrial enzyme methylmalonyl-CoA mutase. In humans, the
298 product of this gene is a vitamin B12-dependent enzyme that catalyzes the isomerization of
299 methylmalonyl-CoA to succinyl-CoA. A previous study has shown that vitamin B12 modulates
300 telomere integrity by oxidative stress pathway⁴⁸, but the causal correlation between *MMUT*
301 and TL is unknown. We also found that *MMUT* knockdown in most monoclonal HTR8/SVneo
302 lines significantly reduced TL (Fig. 5D and 5E). With continuous passage, the TL of the
303 shMMUT-1-2 monoclonal cell line shortened continually (Fig. 5F). In addition, the inhibition
304 of the other two new genes *KIAA1429* (a vital component of the m6A methyltransferase
305 complex) and *YWHAZ* (tyrosine3-monooxygenase/tryptophan 5-monooxygenase activation
306 protein zeta) showed a similar pattern of telomere shortening (Fig. 5G–J). This functional
307 validation greatly supports the causal association between these enzymes and TL maintenance.

308

309 **Incorporating genetic and transcriptomic information for accurate TL prediction**

310 This study, together with previous GWAS findings, has strengthened the polygenic basis of
311 TL variation, yet the genetic determinants for TL explained by all genome-wide variants were
312 not substantial (< 10% variance explained)¹⁰⁻¹². The accurate estimation of TL only relies on
313 a single angle of information, such as genetic or epidemiological factors, which shows a low
314 agreement with actual TL measured by different biochemical assays^{16,49}. To improve the
315 performance of TL prediction and facilitate TL-related clinical applications^{50,51} when
316 accurate TL measurement (such as TRF-based or fluorescent in situ hybridization
317 (FISH)-based test) is absent, we incorporated transcriptomic information of placental tissue
318 into TRF-based RTL prediction model and systematically compared it to the existing
319 strategies. First, an elastic net regression model was constructed on our 166 placental
320 multi-omics data and individual demographic information. Next, we inspected the ability of
321 TL inference using transcriptional risk score (TRS)^{52,53} over static PRS. As a result, the TRS
322 model based on genes regulated by variants linked to TL ($r = 0.64$, P -value = 1.38e-20,
323 10-fold cross-validation) outperformed the PRS-based model ($r = 0.32$, P -value = 3.17e-05) in
324 predicting placental RTL (Fig. 6A and 6B), suggesting that transcriptomic information reflects
325 an additional layer of TL determinants than solely genetic information. Since both PRS- and
326 TRS-based models largely depend on GWAS significant variants, we investigated whether
327 incorporating expression signatures from a specific number of genes could enhance the
328 performance of TL prediction. Thus, the elastic net regression was applied to model the
329 TRF-based RTLs of 166 placentas alone with individual PRS and gender information,
330 resulting in 32 selected genes, independent of PRS, which showed non-zero and significant
331 coefficients (see Methods for details) and found that TL prediction model building on
332 transcriptomic score calculated from the expression of these 32-gene signature (TS-32Gene)
333 suppressed the TRS-based model ($r = 0.69$, P -value = 3.18e-24) (Fig. 6B). Additionally, the
334 network enrichment analysis by EviNet⁵⁴ showed that both signature genes and TL-causal
335 genes were enriched in DNA replication signaling pathway (Supplementary Fig. 12), indicating
336 that TS-32Gene represents a unique and powerful predictor of TL. To further gain predictive
337 performance, we combined transcriptomic signature and genetic determinants of TL on several
338 full models training. Notably, the combination model of TS-32Gene, PRS, and TRS exhibits
339 the best performance ($r = 0.85$, P -value = 1.70e-47) among all trained models (Fig. 6B).

340 To evaluate the validity of TRF-based RTL prediction model independently, we applied the
341 most practical model (with parsimonious information) only based on TS-32Gene and PRS to
342 GTEx multi-omics data and observed a good agreement between the predicted and observed
343 RTL measured by Luminex-based assay across different GTEx tissues (Fig. 6C, $r = 0.26$,
344 P -value = 5.92e-45), especially in whole blood, ovary, and esophagus tissues (Supplementary
345 Table 9). This result not only demonstrated the generalizability of our TL prediction model in
346 different contexts but also implied a shared pattern of TL regulation between the placenta and

347 other tissues. In addition, TL estimated by TelSeq⁵⁵, a sequencing-based TL measurement (see
348 Methods for details), showed a weak correlation with Luminex-derived TL in GTEx whole
349 blood tissues (Fig. 6D, $r = 0.13$, P -value = 0.006), further indicating the superiority of our
350 strategy.

351

352 Discussion

353 Telomere shortening is a classical hallmark of cell senescence and aging, and there are many
354 known elements that contribute to the individual variations of TL, such as genetic,
355 environmental, and lifestyle factors². Although several large-scale GWASs have identified a
356 large number of genetic loci associated with TL^{11,12,32}, however, the true causal genes
357 underlying the telomere content regulation are yet to be elucidated. By leveraging TRF assay,
358 genotyping chip, and RNA-seq on hundreds of placenta samples together with trans-ancestral
359 TL GWAS and functional validations, we systematically investigated the causal genes and
360 developed a powerful prediction model for human TL.

361 A recent study by GTEx consortium has investigated the determinants of TL across various
362 adult human tissues and cell types¹⁶. However, samples included in GTEx experienced
363 life-course exposures to the external environment and physiological status. The inherently short
364 or long TL might be largely determined at birth and may be crucial for lifelong health²⁷.
365 Studies on TL of human tissues with a primitive state are lacking. The placenta embeds in the
366 maternal uterus, allowing nutrition delivery and promoting the growth and development of the
367 fetus⁵⁶. In addition, heritability estimates on adults are often affected by environmental factors,
368 impeding the identification of the true genetic determinants. Since newborn TL could predict
369 later life TL⁵⁷, it is critical to investigate TL determinants of the newborn. However, no
370 existing study has harnessed a significant number of early samples without postnatal
371 environmental exposure to study TL.

372 In the placenta, the telomere is less affected by extraplacental exposure or other non-genetic
373 effects, which provide an ideal proxy for studying the genetic determinants and causal genes of
374 TL. Using the TRF measurement, we are able to not only calculate the mean TL, but also
375 characterize the STP. Next, we found that placental RTL and STP were significantly correlated
376 with genes involved in the ALT pathway but not with telomerase subunit genes. ALT extends
377 the telomeres based on DNA recombination but in a telomerase-independent manner⁵⁸. ATRX
378 interacts with DAXX promoting H3.3 deposition, and participates in DNA replication,
379 genomic stability maintenance, and telomere function maintenance⁵⁹. ATRX gene represses
380 ALT, suggesting the role of ALT repression in determining placental RTL. Besides, we
381 observed low expression levels of telomerase genes, including *TERC* and *TERT*. This was
382 consistent with previous findings^{60,61} that high ALT activity is associated with low or no
383 telomerase activity. The current results emphasized the importance of genes involved in the
384 ALT pathway in telomere function and length maintenance. Furthermore, we observed a

385 discrepancy in RTL characteristics between the placenta and other adult human tissues.
386 Consistent with previous studies, the present study revealed that placental RTL exhibits
387 intra-tissue homogeneity but is longer than other somatic adult tissues^{23,24,62}. Nevertheless, the
388 placental RTL of male infants is slightly longer than that of female infants, while RTL is longer
389 in females than males in adult tissues, suggesting that the females may sustain long RTL during
390 postnatal developments.

391 Studies from multiple worldwide cohorts were pooled to perform trans-ancestral GWAS
392 meta-analysis in over 500,000 individuals. The power to detect genome-wide significant
393 signals associated with TL was improved; as a result, we could detect 20 novel genetic
394 associations and recover 87% of the previously reported TL GWAS significant loci. Notably,
395 PRSs of 166 placental samples constructed by TL-associating variants identified via
396 trans-ancestral GWAS were significantly associated with RTL. However, when evaluating
397 PRSs using either GWAS variants from single cohort or genotypes from GTEx whole
398 blood/UKBB leukocyte samples, we only detected weaker RTL correlations, suggesting that
399 leveraging the trans-ancestral GWAS and TRF-based TL measurement could boost the
400 predictive power of PRS on TL. On the other hand, gene expressions in placental tissue are
401 less perturbed through lifetime exposures. Based on genotype and transcriptome profiling
402 from 166 placental samples, we conducted genome-wide *cis*-eQTL mapping and performed
403 TL-causal gene discovery together with our trans-ancestral GWAS results. Complementary
404 statistical methods (such as COLOC, Fusion-TWAS, and SMR) yield 31 likely causal genes
405 related to TL, and some are rarely or inadequately associated with TL, such as *MMUT*, *RRM1*,
406 *KIAA1429*, and *YWHAZ*, which showed a positive regulation of TL. By establishing
407 HTR8/SVneo cell lines with a stable knockdown of these four genes, we validated their
408 functional relevance in maintaining TL via TRF assay. However, the biological mechanisms
409 and tissue/cell-type specificity of these novel TL-causal genes still need an in-depth
410 investigation in the future. Supposedly, some causal genes may not have been detected in this
411 study due to the limitations of sample size, population difference, and tissue specificity of TL
412 maintenance and regulation.

413 Although TRF assay is a gold standard to quantify TL, it also has many drawbacks; it is
414 time-consuming, less cost-effective, and requires large DNA material⁶³. Since the
415 fine-grained determinants of placental TL could be explored effectively using both genetic and
416 transcriptomic information, we constructed several TL prediction models and systematically
417 compared them to the existing strategies. The proposed model relying on transcriptomic
418 signature not only exhibited a great performance in our TRF-based data but also generalized
419 well in the GTEx data. Our model performs better than a WGS-based TL estimation method,
420 TelSeq. The gained performance in the independent datasets, especially in whole blood, lung,
421 and esophagus tissues, highlighted that the regulators of placental TL might have similar
422 biological roles in other tissues. Thus, we speculated that our TL prediction strategy could
423 assist the TL-related clinical applications^{50,51} when accurate TL measurement (such as
424 TRF-based or FISH-based test) is not reachable.

426 **Methods**

427 **Sample collection and processing**

428 The healthy singleton Chinese pregnancies (n = 166) were recruited prior to delivery at Tianjin
429 Central Hospital of Gynecology Obstetrics, China. These study participants did not have any
430 recorded medical disorders or adverse pregnancy outcomes. The hospital ethics committees
431 approved the collection and use of human placental samples (approval no. 2022KY071). All
432 participants provided written informed consent before sample collection. Placentas were
433 treated within 10□ min of a vaginal delivery from full-term pregnancies (37⁺⁰–41⁺⁶ weeks). The
434 average age of the participants was 32 ±4.0 years, and no tobacco-smoking or alcohol-drinking
435 behavior was noted. The cohort comprised 73 female and 93 male infants. No significant
436 differences were observed in maternal age, maternal BMI, infant weight, and gestation weeks
437 with regard to infant gender ($P > 0.05$).

438 Placental full-thickness biopsies of 1.5 × 1.5□cm were collected from the standardized regions
439 at a distance of 2□cm from the umbilical cord. The placenta was placed with the fetal side
440 upwards and orientated with the largest umbilical cord artery on the fetal side of the placenta as
441 a reference location. To avoid contamination by non-target origin cells, the membranes were
442 cut away, and excess blood was removed using sterile filter paper. To analyze the possible
443 intraplacental variation of TL, all the processed biopsies were divided into three parts and
444 sampled at the fetal and maternal layers to obtain eight samples of each placenta, as described
445 by Wyatt et al. ⁶⁴. All samples were stored in RNAlater at –80 °C until extraction.

446

447 **TRF length analysis**

448 TRF method combined with pulsed-field electrophoresis was used to detect the TL length of
449 166 placental tissues. Genomic DNA isolation kit (Biomiga, BW-GD2211-02) was used to
450 extract genomic DNA from placental tissue and HTR8/SVneo cells in the following
451 experiments. TRF length analysis was applied to measure the TL of these DNA samples.
452 Briefly, 1 µg genomic DNA of each sample was digested with *HinfI* and *RsaI* and then analyzed
453 by agarose gel electrophoresis in 0.5× TBE. Pulsed-field gels [1% (wt/vol)] was run at 6 V,
454 14 °C for 16 h, and normal electrophoresis gels [0.8% (wt/vol)] were run at 100V, 0–4 °C for 3
455 h. Subsequent procedures, such as gel depurination, gel denaturation, gel neutralization, DNA
456 transfer to membrane, hybridization with DIG-labeled telomere probe, chemiluminescent
457 detection, and TRF length analysis, were conducted. The sequence of telomere probe is
458 TAACCCTAACCTAACCTAACCC. As an internal control, HeLa cell DNA was added in
459 the first lane of each experiment to correct for batch-to-batch variation, and the RTL of 166
460 placental tissues was estimated by the ratio of their TL vs. HeLa DNA's TL. Besides, we also
461 consider the telomere < 5000 bp as the short telomere and the ratio of the band's intensity <

462 5000 bp to the total intensity of the entire telomere band as the STP. The quantification and
463 normalization of TRF length were performed using TeloTool⁶⁵.

464

465 **Genotyping, imputation, and quality control**

466 Placental samples were genotyped using the Asian Screening Array (ASA) 750k platform, an
467 Illumina whole-genome single nucleotide polymorphism (SNP) chip designed based on a
468 large-scale East Asian whole-genome sequencing data that encompasses about 750,000
469 markers. Genotype calling by ASA resulted in a dataset of 166 individuals typed at 738,980
470 markers. Data cleaning was performed using PLINK v1.9⁶⁶. All genotyped variants were
471 subjected to quality control (QC) before imputation. Consequently, variants with (1) call rate (<
472 95%) in all samples, (2) minor allele frequency (MAF) < 0.0001, and (3) departures from
473 Hardy-Weinberg equilibrium ($p < 1E-5$) were removed. Also, individuals with the following
474 criteria were removed: (1) overall SNP genotyping call rate < 95% and heterozygosity rate > 3
475 SD; (2) genetically inferred sex mismatches between genotype and self-report; (3) related
476 individuals with an identity-by-descent value > 0.1875; Before imputation, we removed SNPs
477 with C/G and A/T alleles to avoid strand flipping. Then, we used Michigan Imputation Server⁶⁷
478 to impute untyped SNPs by borrowing the LD information from all samples using GAsP with
479 Minimac4 for imputation and Eagle v2.4 for phasing. Following imputation, any imputed
480 variant with an imputation quality score < 0.3 or MAF < 0.01 was removed.

481

482 **Transcriptome profiling and quantification**

483 During DNA genotyping and TL measurement, we performed RNA-seq to quantify the
484 genome-wide mRNA expression for 166 placental samples. An equivalent of 3 μ g RNA per
485 sample was used as an input material for the RNA sample preparations. RNA-seq was
486 performed using the Illumina NEBNext[®] UltraTM RNA sample preparation protocol. The final
487 libraries were sequenced on HiSeq 4000 platform using 150 bp paired-end chemistry and was
488 run with a coverage goal of 80M reads. Reads containing adapter and ploy-N and those with
489 low quality were removed from raw sequencing reads using fastp⁶⁸. Sequencing QC was used
490 to obtain the overall quality, GC content, and adapter contamination using FastQC
491 (<http://www.bioinformatics.babraham.ac.uk/projects/fastqc>). Then, we used STAR v2.5.3a⁶⁹
492 to align the paired-end reads to the reference genome. Gene annotation file was downloaded
493 from GENCODE release 26 (https://www.gencodegenes.org/human/release_26.html).
494 RNA-SeqQC v1.1.9⁷⁰ was applied to count the read numbers mapped to each gene. The genes
495 were selected based on the following expression thresholds: ≥ 0.1 TPM and ≥ 6 reads count in
496 at least 20% of samples.

497

498 **Co-expression network construction**

499 We used WGCNA ²⁹ to construct the co-expression modules and calculate the gene
500 connectivities. The co-expression networks were constructed with the soft power at 9, while
501 other parameters were set at default. The adjacency was transformed into a topological overlap
502 matrix (TOM), and the average linkage hierarchical clustering was performed according to the
503 TOM-based dissimilarity measure. The module eigengene (ME) was the first principal
504 component of a given module and could be considered a representative of the module's gene
505 expression profile. The 26 MEs for the 26 distinct modules were each tested for the correlations
506 with RTL. Then, gene connectivities were determined by calculating the connectivity values
507 using softConnectivity function of WGCNA. Briefly, connectivity describes how strongly a
508 gene is connected to all the other genes in the network. The absolute value of Pearson's
509 correlation coefficient was calculated for all pairwise comparisons of gene expression values
510 across all samples. The Pearson's correlation matrix was then transformed into an adjacency
511 matrix. softConnectivity constructed the adjacency matrix and calculated the connectivity of
512 each gene, i.e., the sum of the adjacency to the other genes. A total of 4679 genes exhibiting the
513 top 30% high expression variance (captures more valid information) were selected for the
514 co-expression analysis. K-means clustering was used to determine the gene groups for the
515 connectivity shift. We also determined the number of clusters by Elbow method. Finally, GO
516 enrichment analysis was carried out via R package clusterProfiler⁷¹.

517

518 **eQTL mapping**

519 The expression values for each gene were further inverse normal transformed across samples
520 by trimmed mean of M-values ⁷². eQTL mapping was performed using tensorQTL⁷³, a
521 GPU-based method with high efficiency. Next, we used a linear regression model, with top 5
522 genotype principal components (PCs), age, and 30 PEER factors adjusted. Genotype PCs were
523 computed based on the post-QC genotyping VCF using EIGENSTRAT⁷⁴. To detect *cis*-eQTLs
524 effects, we tested the nominal associations between all variant-gene pairs within a ± 1 Mb
525 window around the TSS of each gene and estimated the beta-approximated empirical *P*-values
526 to obtain appropriate significance thresholds based on 10,000 permutations of each gene.
527 Multiple testing corrections were assessed using the Benjamini–Hochberg algorithm, with FDR
528 across all *cis*-eQTL tests within each chromosome estimated. The placental chromatin state
529 regions predicted by chromHMM ³⁴ 15-core state model were downloaded from
530 <https://egg2.wustl.edu/roadmap/>. We performed Fisher's exact test to investigate whether
531 eQTLs were prone to be located in a specific chromatin state than expected. A two-sided
532 *P*-value and odds ratio were calculated to measure the enrichment of eQTLs in the chromatin
533 state regions.

534

535 **GWAS meta-analysis**

536 We collected genome-wide summary statistics from three TL trait GWASs based on large-scale
537 individuals, including SCHS ¹⁰, NHLBI TOPMed ¹², and UK Biobank (UKBB) ¹¹. First, the
538 variants with MAF < 0.01 were excluded, and then a fixed-effect meta-analysis weighted by
539 sample size of each study was conducted using METAL ⁷⁵. Genome-wide statistical
540 significance for the meta-analysis was set at $p < 5E-8$, HETEROGENEITY mode was set to
541 determine whether the observed effect sizes were heterogeneous across samples. To recognize
542 the novel genetic loci in trans-ancestral meta-analyses, we first identified the associated genetic
543 loci in TOPMed, UKBB, and SCHS meta-analyses at a threshold of $p < 5E-8$. A locus was
544 defined novel in a trans-ancestral meta-analyses if it did not overlap with any loci of GWAS
545 from a single cohort. Manhattan and Q-Q plots were generated by CMplot ⁷⁶. In order to
546 identify the positions of loci containing TL-associated variants, linkage disequilibrium (LD)
547 clumping was conducted using PLINK v1.9. The variants were pruned with the following
548 parameters: a P -value cutoff of 5E-8, at a genomic distance of 10 Mb, and $R^2 < 0.001$ with
549 the lead SNP, using the LD structure of the 1000 Genomes Project as a reference panel.

550

551 **PRS analysis**

552 Polygenic scores of TL were constructed using PRSice-2 ⁷⁷ to gauge the associations between
553 reported variations of TL in general populations and in the current study. The scores were
554 computed as the weighted sum of effect allele dosages, as a matrix multiplication of SNP
555 dosages per individual by betas per SNP, i.e., the outcome is a single score of each individual's
556 genetic loading for TL. Our measure of predictive power is the incremental R^2 from adding the
557 score to a regression of the phenotype while adjusting for top five genotyping PCs, sex, and
558 maternal age. The PRS was calculated by summing over all SNPs meeting a set of thresholds,
559 respectively. The null P -value of the association of the best-fit GWAS P -value threshold was
560 converted to the empirical P -value under 10,000 permutations. Pearson's correlations between
561 PRS and RTL were used to compare the PRS analytical performance for the Chinese samples in
562 UKBB, all samples in GTEx, and all samples in this study.

563

564 **Colocalization analysis**

565 COLOC was applied to colocalize eQTL and TL signals which provided evidence of a putative
566 causal correlation between the eQTL target gene and TL ³⁵. Herein, we used coloc.abf function
567 implemented in the R package COLOC to perform colocalization analysis. The colocalization
568 with $P4 > 0.5$ was used as a threshold for colocalized signals. The regional plot was generated

569 using locuszoom (<http://locuscompare.com/>)⁷⁸, and LD was calculated based on the genotype
570 of all individuals from 1000 Genomes project phase3⁷⁹.

571

572 **TWAS analysis**

573 The summary-based TWAS was applied for GWAS meta-analysis data using FUSION
574 following the pipeline described on their website (<http://gusevlab.org/projects/fusion>)³⁶.
575 FUSION estimated the heritability of gene expression levels explained by SNPs in *cis* regions
576 to each gene using the mixed-linear model (for instance, BLUP, BSLMM, LASSO, Elastic Net,
577 and Top1 models). The weights for gene expression in the placenta were calculated based on
578 the correlation between SNPs and the placental gene expression while accounting for LD
579 among SNPs. The genes that failed heritability check (heritability *P*-value > 0.01) were
580 excluded from further analyses. We restricted the *cis*-locus to 500 kb on the either side of the
581 gene boundary. Then, the associations between predicted expression of genes and TL were
582 identified by FUSIOIN at default settings. Finally, the proportion of variance in gene
583 expression, *P*-value, and Z-score was obtained from FUSION. TWAS Manhattan plot was
584 generated using TWAS-plotter (<https://github.com/opain/TWAS-plotter>). TRS was
585 constructed by the genetic value weighted by their Z-score in the TWAS.

586

587 **SMR analysis**

588 The summary-based SMR method allowed us to infer the causal association between
589 genetically determined gene expression and TL. The SMR test was developed to test the
590 association between the exposure and the outcome using a single genetic variant as the
591 instrumental variable³⁷. Based on the assumption of SMR, SNPs are required to affect the TL
592 only through the effects on gene expression. *Cis*-eQTLs were used as the instrumental variables
593 in this analysis. The heterogeneity in dependent instruments (HEIDI) test was carried out to test
594 the existence of linkage in the observed association. Rejecting the null hypothesis (i.e., $P_{HEIDI} <$
595 0.01) indicated the presence of two or more variants in high LD underlying the association.
596 Thus, we used the default settings in SMR (i.e., MAF > 0.01, excluded SNPs with LD R^2
597 between top-SNP > 0.90 and < 0.05 and one of each pair of the remaining SNPs with LD R^2 >
598 0.90), and leveraged the FDR for multiple testing corrections.

599

600 **Elastic net regression**

601 We also used an elastic net regression model to regress TL on maternal age, infant sex, TL PRS,
602 TRS, and gene expressions. It is a regularized regression method that linearly combines the L1

603 and L2 penalties of the LASSO and ridge methods ⁸⁰, emphasizing model sparsity while
604 appropriately balancing the contributions of co-expressed genes. The raw values of all the
605 features are standardized by removing the mean and scaling to the unit variance before training.
606 Optimal regularization parameters were estimated via 10-fold cross-validation. The alpha
607 parameter was set to 0.14, and the lambda value from the best prediction model selected by
608 exhaustive grid search was set to 0.18. The elastic net regression model automatically selected
609 features for building a TL predictor and reported an effect size for each feature. To compare the
610 incremental predictive power of PRS and TRS, we also trained two models that included
611 maternal age, infant sex, and TL PRS only or TRS only. Since our sample size was < 200, we
612 did not leave a testing set for validation but used a 10-fold cross-validation strategy. Instead,
613 GTEx was utilized as an independent validation source, where only GTEx tissues with > 100
614 samples are used for validation. The correlation (R^2) value between the predicted and the true
615 TL across all samples was used to evaluate the accuracy. Moreover, we compared the
616 performance of the elastic net regression model used in this study and a WGS-based TL
617 estimation tool, TelSeq ⁵⁵. The TelSeq tool estimates the average TL using counts of
618 sequencing reads containing a fixed number of telomere signature TTAGGG repeats. A repeat
619 number of 12 and a GC content window of 48–52% was applied in this calculation. TelSeq was
620 also used to estimate the TL for 670 GTEx whole blood samples based on sequence alignment
621 files derived from WGS data, while R^2 between the predicted and the true TL across all samples
622 was used to compare the performance.

623

624 **Cell culture**

625 HEK 293T cells were grown in DMEM (Corning, USA) supplemented with 10% fetal bovine
626 serum (LONSERA, UY) and 1% penicillin-streptomycin. HTR8/SVneo cells were cultured in
627 1640 (Corning) medium containing 10% fetal bovine serum and 1% penicillin-streptomycin.
628 The optimal culture conditions in the incubator were 37 °C, 5% CO₂, and humidity of about
629 95%.

630

631 **shRNA design and plasmid construction**

632 shRNA sequences were introduced into pLKO.1-puro vectors. The targeting sequences for
633 various shRNAs oligos are as follows:
634 shMMUT-1: 5'-CCCTTGTATTCCAAGAGAGAT-3';
635 shRRM1-1: 5'CCCACAACTTCTAGCTGTTT-3';
636 shRRM1-2: 5'-GCTGTCTCTAACATTGCACAAA-3';
637 shKIAA1429-1: 5'-CGGAATATGAAGCAACAAATT-3';
638 shKIAA1429-2: 5'-CGCTGAGCAAAGTTCTCATAT-3';
639 shYWHAZ-1: 5'-GCAGAGAGCAAAGTCTTCTAT-3';

640 shYWHAZ-2: 5'-GCAATTACTGAGAGACAACTT-3';
641 shUBE2R2-1: 5'-CCAATGTCGATGCTTCAGTTA-3';
642 shScramble: 5'-CCTAAGGTTAAGTCGCCCTCG-3'.

643

644 **Establishment of stable cell lines**

645 shRNA plasmids were transfected into HEK 293T cells with polyethylenimine (PEI),
646 according to the manufacturer's instructions. Lentiviral particles produced by HEK 293T cells
647 were released into the DMEM medium. At 48 and 72 h, the lentiviral particle-containing
648 medium was collected and filtered using a 0.45 µm Syringe Filter Unit. HTR8/SVneo cells
649 were cultured in a 6-well plate (400,000 cells/well) for 24 h to achieve 70–80% confluence at
650 the time of infection by 2 mL lentiviral particle-containing medium. After one day
651 post-infection, 2 days of puromycin selection (2 µg/mL), and knockdown determination, single
652 cells were picked and seeded into 96-well plates to generate monoclonal cell lines.

653

654 **Determination of knockdown by quantitative polymerase chain reaction (qPCR)**

655 When infection and puromycin selection of HTR8/SVneo cells were completed or monoclonal
656 cells from 96-well plates were transferred to 6-well plates, total RNA was extracted using the
657 Eastep® Super Total RNA Extraction Kit (Promega). An equivalent of 1 µg of RNA was reverse
658 transcribed to synthesize cDNA using HiScript® II Q Select RT SuperMix (Vazyme Biotech).
659 Then, 25 ng of cDNA was used as a template for qPCR analysis with ChamQ Universal SYBR
660 qPCR Master Mix (Vazyme Biotech). The forward and reverse primers for qPCR are listed
661 below:

662 *qMMUT-F*: 5'-CAGTTGGAAAAGAAGACGCTGTA-3';
663 *qMMUT-R*: 5'-ATCTGCCTGTTCGCACTGA-3';
664 *qRRM1-F*: 5'-ACTAAGCACCTGACTATGCTATCC-3';
665 *qRRM1-R*: 5'-CTTCCATCACATCACTGAACACTTT-3';
666 *qKIAA1429-F*: 5'-GTTGTGCCACCACCAAGAGG-3';
667 *qKIAA1429-R*: 5'-AACCCACCACGGGAAGAAAT-3';
668 *qYWHAZ-F*: 5'-AGCCATTGCTGAACTTGATACA-3';
669 *qYWHAZ-R*: 5'-AATTTCCCTCCTTCTCCTG-3';
670 *qGAPDH-F*: 5'-TGACAAACGAATTGGCTACA-3';
671 *qGAPDH-R*: 5'-GTGGTCCAGGGGTCTTACTC-3'.

672

673 **Data Availability**

674 Processed RNA-seq data, full summary statistics of eQTL and GWAS meta-analysis will be
675 deposited into public repository. The full GWAS summary statistics for UKBB were obtained
676 from <https://figshare.com/s/caa99dc0f76d62990195>. Individual-level genotype data are
677 available by application to the UKBB (<https://www.ukbiobank.ac.uk/register-apply/>). The full
678 GWAS summary statistics for TOPMed were applied from the database of Genotypes and
679 Phenotypes (dbGaP), under accession phs001974.v3.p1. The full GWAS summary statistics for
680 SCHS were obtained from <https://doi.org/10.6084/m9.figshare.8066999>. TRF-based TL
681 measurement of placenta samples are available upon request. TL of various tissues in GTEx
682 were downloaded from (<https://www.gtexportal.org/home/datasets>). The WGS data of GTEx
683 Whole blood samples were applied from dbGaP, under accession phs000424.v8.p2.

684

685 **Acknowledgements**

686 This study was supported by the National Natural Science Foundation of China (Grant
687 Numbers 32270717, 32070675, 32170762, 82001579) and the Tianjin Committee of Science
688 and Technology (Grant Numbers 19JCJQJC63600 and 20JCYBJC01400), and Tianjin Key
689 Laboratory of Human Development and Reproductive Regulation (2019XHY06 and
690 2019XHY07).

691

692 **Competing interests**

693 The authors declare no conflict of interest.

694

695 **Contributions**

696 M.J.L., F.W. and Y.C. conceived of the project. Y.Z., J.Z. and D.H. performed the experiments
697 and analyses. W.L., J.C., Y.S., X.F., H.Y., X.D. and X.Y. contributed the data collection and
698 processing. L.S., L.S., Z.L., J.Y., J.H. and K.C. contributed to manuscript polishing and
699 provided analysis suggestions. M.J.L., Y.Z., F.W., Y.C. and J.Z. wrote the manuscript. All
700 authors read and approved the final submission.

701

702 **Figure Legends**

703 **Figure 1. Placental material extraction and measurement.** (A) Schematic depicts the
704 collection procedures of placental samples. (B) Workflow of analysis in this study. TRF
705 analysis, genotyping, and RNA-seq were conducted simultaneously for each sample. (C) TL of
706 different sets from the same placental tissue was analyzed by TRF with regular electrophoresis
707 gels. (D) Distribution of RTL across placenta and 24 GTEx tissue types, dashed line indicates
708 the mean RTL in placenta. (E) Scatter plot shows the correlations between short TL and RTL,
709 with a simple linear regression line fitted.

710 **Figure 2. Trans-ancestral TL GWAS and PRS analysis.** (A) Manhattan plot of various TL
711 GWASs and GWAS meta-analysis. The x-axis represents the genome in physical order; the
712 y-axis shows -log10 *P*-values for all variants. (B) The quantile-quantile (Q-Q) plot compared
713 the *P*-values generated from this fitted distribution against the observed *P*-values. (C)
714 LocusZoom plot for regional associations of a locus associating with TL in *SWI1* gene, SNPs
715 are colored according to their LD with the lead SNP, rs10798002. The left y-axis shows
716 association *P*-values on the -log10 *P*-values for all SNPs in this locus, the right y-axis shows the
717 recombination rate and the x-axis shows the chromosomal position. The bottom of plot shows
718 the near genes. (D) Dot plot of GO enrichment for the nearest genes of TL-associated variants.
719 (E) Scatter plot for RTL vs. PRSs with a simple linear regression line fitted in this study, GTEx,
720 and UKBB.

721 **Figure 3. Gene expression patterns of placental TL maintenance.** (A) Scatter plots shows
722 the associations between RTL and *TPP1*. (B) Scatter plots shows the associations between RTL
723 and genes involved in ALT pathway. (C) Scatter plots shows the associations between short TL
724 and *TPP1*. (D) Scatter plots shows the associations between short TL and genes involved in the
725 ALT pathway. (E) Dendrogram of module eigengenes based on dissimilarity measure (1-TOM)
726 and the associations between each module and TL. (F) Heatmap of the connectives for
727 high-variance genes based on about 25% of samples, while the left-most is based on samples
728 with upper-quartile TLs, and the right-most is based on samples with lower-quartile TLs, lower
729 score represents a low overlap and larger score represents a high overlap between the genes. (G)
730 Dot plot of GO enrichment for genes clusters that predominately have higher connectives in
731 samples with long TL (upper) or short TL (bottom).

732 **Figure 4. Causal associations between genetically determined gene expressions and TL.**
733 (A) Manhattan plot of transcriptome-wide association results. The x-axis represents the
734 genome in physical order; the y-axis shows Z score for all genes. Genes that passed multiple
735 testing corrections (FDR < 0.1) are highlighted in red and labeled with gene name. (B–E)
736 LocusCompare plots for the (B) *MMUT*, (C) *RRM1*, (D) *KIAA1429*, and (E) *YWHAZ* loci,
737 where the GWAS signals (x-axis) colocalized the eQTL signals (y-axis). LD is colored with
738 respect to the GWAS lead SNPs. (F–I) Scatter plot of the effect sizes of variants reported in TL
739 GWAS and placental eQTLs from (F) *MMUT*, (G) *RRM1*, (H) *KIAA1429*, and (I) *YWHAZ*.

740 Effect sizes of the variants in the TL GWAS (y-axis) and eQTL (x-axis) are plotted. Error bars
741 indicate 95% confidence interval.

742 **Figure 5. Experimental validation of TL regulation by perturbing expression of *MMUT*,**

743 *RRM1*, *KIAA1429*, and *YWHAZ*. (A) 34 days after HTR8/SVneo cells were infected with
744 shRRM1 lentiviral particles, 8 shRRM1 monoclonal cell lines grown in 96-well plates were
745 transferred to 6-well plates. TRF assay was used to measure the TL of these cell lines. (B)
746 *RRM1* RNA levels were estimated by qPCR and analyzed by GraphPad Prism software version
747 6.0. Data are represented as mean \pm SD; n = 3. ****P < 0.0001. (C) HTR8/SVneo cells stably
748 expressing control (shScramble) and shRRM1 were passaged over time (DAY) and examined
749 for average TL by TRF. (D) 34 days after HTR8/SVneo cells were infected with shMMUT
750 lentiviral particles, six shMMUT monoclonal cell lines grown in 96-well plates were
751 transferred to 6-well plates. TL of these six cell lines was measured by TRF assay. (E) *MMUT*
752 RNA levels were estimated by qPCR and analyzed by GraphPad Prism software version 6.0.
753 Data are represented as mean \pm SD; n=3. ***P < 0.001; ****P < 0.0001. (F) HTR8/SVneo cells
754 stably expressing control (shScramble) and shRNA sequences against MMUT were passaged
755 over time (DAY) and examined for average TL by TRF. (G) 32 days after infection of
756 shKIAA1429 lentiviral particles, six shKIAA1429 monoclonal cell lines from 96-well plates
757 were grown in 6-well plates. The TL of these cell lines was measured by TRF assay. (H)
758 *KIAA1429* RNA levels were tested by qPCR and analyzed by GraphPad Prism software version
759 6.0. Data are represented as mean \pm SD; n = 3. ****P < 0.0001. (I) 32 days after infection of
760 shYWHAZ lentiviral particles, 5 shYWHAZ monoclonal cell lines grew from 96-well plates to
761 6-well plates. TL of these cell lines was measured by TRF assay. (J) *YWHAZ* RNA levels were
762 estimated by qPCR and analyzed by GraphPad Prism software version 6.0. Data represent
763 mean \pm SD; n=3. ****P < 0.0001.

764 **Figure 6. Performance of placental TL prediction model.** (A) Scatter plot shows the actual
765 TL values in placenta against the values predicted by the model. (B) Bar chart for performance
766 of elastic net models based on different feature combinations. (C) Scatter plot shows the
767 correlations between TelSeq and TQImean for GTEx whole blood individuals with a simple
768 linear regression line fitted. (D) Scatter plot shows the actual TL values in GTEx tissues against
769 those predicted by the model, only GTEx tissues with >100 samples were used for validation.
770 Dots are colored according to their tissue types.

771

772

773

774

775 References

776 1 McEachern, M. J., Krauskopf, A. & Blackburn, E. H. Telomeres and their control. *Annu
777 Rev Genet* **34**, 331-358, doi:10.1146/annurev.genet.34.1.331 (2000).

778 2 Blackburn, E. H., Epel, E. S. & Lin, J. Human telomere biology: A contributory and
779 interactive factor in aging, disease risks, and protection. *Science* **350**, 1193-1198,
780 doi:10.1126/science.aab3389 (2015).

781 3 von Zglinicki, T. Oxidative stress shortens telomeres. *Trends Biochem Sci* **27**, 339-344,
782 doi:10.1016/s0968-0004(02)02110-2 (2002).

783 4 Fasching, C. L. Telomere length measurement as a clinical biomarker of aging and
784 disease. *Crit Rev Clin Lab Sci* **55**, 443-465, doi:10.1080/10408363.2018.1504274
785 (2018).

786 5 Vaiserman, A. & Krasnienkov, D. Telomere Length as a Marker of Biological Age:
787 State-of-the-Art, Open Issues, and Future Perspectives. *Front Genet* **11**, 630186,
788 doi:10.3389/fgene.2020.630186 (2020).

789 6 Rossiello, F., Jurk, D., Passos, J. F. & d'Adda di Fagagna, F. Telomere dysfunction in
790 ageing and age-related diseases. *Nat Cell Biol* **24**, 135-147,
791 doi:10.1038/s41556-022-00842-x (2022).

792 7 Andreu-Sanchez, S. *et al.* Genetic, parental and lifestyle factors influence telomere
793 length. *Commun Biol* **5**, 565, doi:10.1038/s42003-022-03521-7 (2022).

794 8 Njajou, O. T. *et al.* Telomere length is paternally inherited and is associated with
795 parental lifespan. *Proc Natl Acad Sci U S A* **104**, 12135-12139,
796 doi:10.1073/pnas.0702703104 (2007).

797 9 Slagboom, P. E., Droog, S. & Boomsma, D. I. Genetic determination of telomere size
798 in humans: a twin study of three age groups. *Am J Hum Genet* **55**, 876-882 (1994).

799 10 Dorajoo, R. *et al.* Loci for human leukocyte telomere length in the Singaporean
800 Chinese population and trans-ethnic genetic studies. *Nat Commun* **10**, 2491,
801 doi:10.1038/s41467-019-10443-2 (2019).

802 11 Codd, V. *et al.* Polygenic basis and biomedical consequences of telomere length
803 variation. *Nat Genet* **53**, 1425-1433, doi:10.1038/s41588-021-00944-6 (2021).

804 12 Taub, M. A. *et al.* Genetic determinants of telomere length from 109,122 ancestrally
805 diverse whole-genome sequences in TOPMed. *Cell Genom* **2**, 100084,
806 doi:10.1016/j.xgen.2021.100084 (2022).

807 13 Astuti, Y., Wardhana, A., Watkins, J., Wulaningsih, W. & Network, P. R. Cigarette
808 smoking and telomere length: A systematic review of 84 studies and meta-analysis.
809 *Environ Res* **158**, 480-489, doi:10.1016/j.envres.2017.06.038 (2017).

810 14 Topiwala, A. *et al.* Alcohol consumption and telomere length: Mendelian
811 randomization clarifies alcohol's effects. *Mol Psychiatry*,
812 doi:10.1038/s41380-022-01690-9 (2022).

813 15 Werner, C. M. *et al.* Differential effects of endurance, interval, and resistance
814 training on telomerase activity and telomere length in a randomized, controlled
815 study. *Eur Heart J* **40**, 34-46, doi:10.1093/eurheartj/ehy585 (2019).

816 16 Demanelis, K. *et al.* Determinants of telomere length across human tissues. *Science*
817 **369**, doi:10.1126/science.aaz6876 (2020).

818 17 Bou Sleiman, M. *et al.* Sex- and age-dependent genetics of longevity in a
819 heterogeneous mouse population. *Science* **377**, eabo3191,
820 doi:10.1126/science.abo3191 (2022).

821 18 Yamamoto, R. *et al.* Tissue-specific impacts of aging and genetics on gene expression
822 patterns in humans. *Nat Commun* **13**, 5803, doi:10.1038/s41467-022-33509-0
823 (2022).

824 19 Barbeira, A. N. *et al.* Exploiting the GTEx resources to decipher the mechanisms at
825 GWAS loci. *Genome Biol* **22**, 49, doi:10.1186/s13059-020-02252-4 (2021).

826 20 Wainberg, M. *et al.* Opportunities and challenges for transcriptome-wide association
827 studies. *Nat Genet* **51**, 592-599, doi:10.1038/s41588-019-0385-z (2019).

828 21 Cano-Gamez, E. & Trynka, G. From GWAS to Function: Using Functional Genomics to
829 Identify the Mechanisms Underlying Complex Diseases. *Front Genet* **11**, 424,
830 doi:10.3389/fgene.2020.00424 (2020).

831 22 Kimura, M. *et al.* Measurement of telomere length by the Southern blot analysis of
832 terminal restriction fragment lengths. *Nat Protoc* **5**, 1596-1607,
833 doi:10.1038/nprot.2010.124 (2010).

834 23 Okuda, K. *et al.* Telomere length in the newborn. *Pediatr Res* **52**, 377-381,
835 doi:10.1203/00006450-200209000-00012 (2002).

836 24 Lin, J. *et al.* Systematic and Cell Type-Specific Telomere Length Changes in Subsets of
837 Lymphocytes. *J Immunol Res* **2016**, 5371050, doi:10.1155/2016/5371050 (2016).

838 25 Allsopp, R. C. & Harley, C. B. Evidence for a Critical Telomere Length in Senescent
839 Human Fibroblasts. *Experimental Cell Research* **219**, 130-136,
840 doi:<https://doi.org/10.1006/excr.1995.1213> (1995).

841 26 Shammas, M. A. Telomeres, lifestyle, cancer, and aging. *Curr Opin Clin Nutr Metab
842 Care* **14**, 28-34, doi:10.1097/MCO.0b013e32834121b1 (2011).

843 27 Factor-Litvak, P. *et al.* Leukocyte Telomere Length in Newborns: Implications for the
844 Role of Telomeres in Human Disease. *Pediatrics* **137**, doi:10.1542/peds.2015-3927
845 (2016).

846 28 Skruzny, M. *et al.* An endoribonuclease functionally linked to perinuclear mRNP
847 quality control associates with the nuclear pore complexes. *PLoS Biol* **7**, e8,
848 doi:10.1371/journal.pbio.1000008 (2009).

849 29 Langfelder, P. & Horvath, S. WGCNA: an R package for weighted correlation network
850 analysis. *BMC Bioinformatics* **9**, 559, doi:10.1186/1471-2105-9-559 (2008).

851 30 Zalzman, M., Meltzer, W. A., Portney, B. A., Brown, R. A. & Gupta, A. The Role of
852 Ubiquitination and SUMOylation in Telomere Biology. *Curr Issues Mol Biol* **35**, 85-98,
853 doi:10.21775/cimb.035.085 (2020).

854 31 Grillari, J., Grillari-Voglauer, R. & Jansen-Dürr, P. in *Protein Metabolism and
855 Homeostasis in Aging* (ed Nektarios Tavernarakis) 172-196 (Springer US, 2010).

856 32 Li, C. *et al.* Genome-wide Association Analysis in Humans Links Nucleotide
857 Metabolism to Leukocyte Telomere Length. *Am J Hum Genet* **106**, 389-404,
858 doi:10.1016/j.ajhg.2020.02.006 (2020).

859 33 Peng, S. *et al.* Expression quantitative trait loci (eQTLs) in human placentas suggest
860 developmental origins of complex diseases. *Hum Mol Genet* **26**, 3432-3441,
861 doi:10.1093/hmg/ddx265 (2017).

862 34 Roadmap Epigenomics, C. *et al.* Integrative analysis of 111 reference human
863 epigenomes. *Nature* **518**, 317-330, doi:10.1038/nature14248 (2015).

864 35 Giambartolomei, C. *et al.* Bayesian test for colocalisation between pairs of genetic
865 association studies using summary statistics. *PLoS Genet* **10**, e1004383,
866 doi:10.1371/journal.pgen.1004383 (2014).

867 36 Gusev, A. *et al.* Integrative approaches for large-scale transcriptome-wide
868 association studies. *Nat Genet* **48**, 245-252, doi:10.1038/ng.3506 (2016).

869 37 Zhu, Z. *et al.* Integration of summary data from GWAS and eQTL studies predicts
870 complex trait gene targets. *Nat Genet* **48**, 481-487, doi:10.1038/ng.3538 (2016).

871 38 Feng, X. *et al.* CTC1-STN1 terminates telomerase while STN1-TEN1 enables C-strand
872 synthesis during telomere replication in colon cancer cells. *Nature Communications*
873 **9**, 2827, doi:10.1038/s41467-018-05154-z (2018).

874 39 Grandin, N., Damon, C. & Charbonneau, M. Ten1 functions in telomere end
875 protection and length regulation in association with Stn1 and Cdc13. *EMBO J* **20**,
876 1173-1183, doi:10.1093/emboj/20.5.1173 (2001).

877 40 Episkopou, H., Diman, A., Claude, E., Viceconte, N. & Decottignies, A. TSPYL5
878 Depletion Induces Specific Death of ALT Cells through USP7-Dependent Proteasomal
879 Degradation of POT1. *Mol Cell* **75**, 469-482 e466, doi:10.1016/j.molcel.2019.05.027
880 (2019).

881 41 Saint-Léger, A. *et al.* The basic N-terminal domain of TRF2 limits recombination
882 endonuclease action at human telomeres. *Cell Cycle* **13**, 2469-2474,
883 doi:10.4161/cc.29422 (2014).

884 42 Gallina, I. *et al.* The ubiquitin ligase RFWD3 is required for translesion DNA synthesis.
885 *Molecular Cell* **81**, 442-458.e449, doi:10.1016/j.molcel.2020.11.029 (2021).

886 43 Brower, C. S. *et al.* Liat1, an arginyltransferase-binding protein whose evolution
887 among primates involved changes in the numbers of its 10-residue repeats.
888 *Proceedings of the National Academy of Sciences* **111**, E4936-E4945,
889 doi:10.1073/pnas.1419587111 (2014).

890 44 Graham, C. H. *et al.* Establishment and characterization of first trimester human
891 trophoblast cells with extended lifespan. *Exp Cell Res* **206**, 204-211,
892 doi:10.1006/excr.1993.1139 (1993).

893 45 Nordlund, P. & Reichard, P. Ribonucleotide reductases. *Annu Rev Biochem* **75**,
894 681-706, doi:10.1146/annurev.biochem.75.103004.142443 (2006).

895 46 Maicher, A. *et al.* Rnr1, but not Rnr3, facilitates the sustained telomerase-dependent
896 elongation of telomeres. *PLoS Genet* **13**, e1007082,
897 doi:10.1371/journal.pgen.1007082 (2017).

898 47 Nersisyan, L., Nikoghosyan, M., Genome of the Netherlands, c. & Arakelyan, A.
899 WGS-based telomere length analysis in Dutch family trios implicates stronger
900 maternal inheritance and a role for RRM1 gene. *Sci Rep* **9**, 18758,
901 doi:10.1038/s41598-019-55109-7 (2019).

902 48 Praveen, G., Sivaprasad, M. & Reddy, G. B. Telomere length and vitamin B12. *Vitam
903 Horm* **119**, 299-324, doi:10.1016/bs.vh.2022.01.014 (2022).

904 49 Puterman, E. *et al.* Lifespan adversity and later adulthood telomere length in the
905 nationally representative US Health and Retirement Study. *Proc Natl Acad Sci U S A*
906 **113**, E6335-E6342, doi:10.1073/pnas.1525602113 (2016).

907 50 Telomeres Mendelian Randomization, C. *et al.* Association Between Telomere
908 Length and Risk of Cancer and Non-Neoplastic Diseases: A Mendelian Randomization
909 Study. *JAMA Oncol* **3**, 636-651, doi:10.1001/jamaoncol.2016.5945 (2017).

910 51 Haycock, P. C. *et al.* Leucocyte telomere length and risk of cardiovascular disease:
911 systematic review and meta-analysis. *BMJ* **349**, g4227, doi:10.1136/bmj.g4227
912 (2014).

913 52 Marigorta, U. M. *et al.* Transcriptional risk scores link GWAS to eQTLs and predict
914 complications in Crohn's disease. *Nat Genet* **49**, 1517-1521, doi:10.1038/ng.3936
915 (2017).

916 53 Liang, Y. *et al.* Polygenic transcriptome risk scores (PTRS) can improve portability of
917 polygenic risk scores across ancestries. *Genome Biol* **23**, 23, doi:10.1186/s13059-021-02591-w (2022).

919 54 Jeggari, A. *et al.* EviNet: a web platform for network enrichment analysis with
920 flexible definition of gene sets. *Nucleic Acids Res* **46**, W163-W170,
921 doi:10.1093/nar/gky485 (2018).

922 55 Ding, Z. *et al.* Estimating telomere length from whole genome sequence data.
923 *Nucleic Acids Res* **42**, e75, doi:10.1093/nar/gku181 (2014).

924 56 Burton, G. J. & Fowden, A. L. The placenta: a multifaceted, transient organ. *Philos
925 Trans R Soc Lond B Biol Sci* **370**, 20140066, doi:10.1098/rstb.2014.0066 (2015).

926 57 Martens, D. S. *et al.* Newborn telomere length predicts later life telomere length:
927 Tracking telomere length from birth to child- and adulthood. *EBioMedicine* **63**,
928 103164, doi:10.1016/j.ebiom.2020.103164 (2021).

929 58 Cesare, A. J. & Reddel, R. R. Alternative lengthening of telomeres: models,
930 mechanisms and implications. *Nat Rev Genet* **11**, 319-330, doi:10.1038/nrg2763
931 (2010).

932 59 Valenzuela, M., Amato, R., Sgura, A., Antoccia, A. & Berardinelli, F. The Multiple
933 Facets of ATRX Protein. *Cancers* **13**, doi:10.3390/cancers13092211 (2021).

934 60 Sung, J. Y., Lim, H. W., Joung, J. G. & Park, W. Y. Pan-Cancer Analysis of Alternative
935 Lengthening of Telomere Activity. *Cancers (Basel)* **12**, doi:10.3390/cancers12082207
936 (2020).

937 61 Sung, J. Y. & Cheong, J. H. Alternative lengthening of telomeres is mechanistically
938 linked to potential therapeutic vulnerability in the stem-like subtype of gastric
939 cancer. *Clin Transl Med* **11**, e561, doi:10.1002/ctm2.561 (2021).

940 62 Allsopp, R., Shimoda, J., Easa, D. & Ward, K. Long Telomeres in the Mature Human
941 Placenta. *Placenta* **28**, 324-327, doi:<https://doi.org/10.1016/j.placenta.2006.04.003>
942 (2007).

943 63 Lai, T. P., Wright, W. E. & Shay, J. W. Comparison of telomere length measurement
944 methods. *Philos T R Soc B* **373**, doi:ARTN 20160451

945 10.1098/rstb.2016.0451 (2018).

946 64 Wyatt, S. M. *et al.* The correlation between sampling site and gene expression in the
947 term human placenta. *Placenta* **26**, 372-379, doi:10.1016/j.placenta.2004.07.003
948 (2005).

949 65 Gohring, J., Fulcher, N., Jacak, J. & Riha, K. TeloTool: a new tool for telomere length
950 measurement from terminal restriction fragment analysis with improved probe
951 intensity correction. *Nucleic Acids Res* **42**, e21, doi:10.1093/nar/gkt1315 (2014).

952 66 Chang, C. C. *et al.* Second-generation PLINK: rising to the challenge of larger and
953 richer datasets. *Gigascience* **4**, 7, doi:10.1186/s13742-015-0047-8 (2015).

954 67 Das, S. *et al.* Next-generation genotype imputation service and methods. *Nat Genet*
955 **48**, 1284-1287, doi:10.1038/ng.3656 (2016).

956 68 Chen, S., Zhou, Y., Chen, Y. & Gu, J. fastp: an ultra-fast all-in-one FASTQ preprocessor.
957 *Bioinformatics* **34**, i884-i890, doi:10.1093/bioinformatics/bty560 (2018).

958 69 Dobin, A. *et al.* STAR: ultrafast universal RNA-seq aligner. *Bioinformatics* **29**, 15-21,
959 doi:10.1093/bioinformatics/bts635 (2013).

960 70 DeLuca, D. S. *et al.* RNA-SeQC: RNA-seq metrics for quality control and process
961 optimization. *Bioinformatics* **28**, 1530-1532, doi:10.1093/bioinformatics/bts196
962 (2012).

963 71 Yu, G., Wang, L. G., Han, Y. & He, Q. Y. clusterProfiler: an R package for comparing
964 biological themes among gene clusters. *OMICS* **16**, 284-287,
965 doi:10.1089/omi.2011.0118 (2012).

966 72 Robinson, M. D. & Oshlack, A. A scaling normalization method for differential
967 expression analysis of RNA-seq data. *Genome Biol* **11**, R25,
968 doi:10.1186/gb-2010-11-3-r25 (2010).

969 73 Taylor-Weiner, A. *et al.* Scaling computational genomics to millions of individuals
970 with GPUs. *Genome Biology* **20**, 228, doi:10.1186/s13059-019-1836-7 (2019).

971 74 Price, A. L. *et al.* Principal components analysis corrects for stratification in
972 genome-wide association studies. *Nat Genet* **38**, 904-909, doi:10.1038/ng1847
973 (2006).

974 75 Willer, C. J., Li, Y. & Abecasis, G. R. METAL: fast and efficient meta-analysis of
975 genomewide association scans. *Bioinformatics* **26**, 2190-2191,
976 doi:10.1093/bioinformatics/btq340 (2010).

977 76 Yin, L. *et al.* rMVP: A Memory-efficient, Visualization-enhanced, and
978 Parallel-accelerated Tool for Genome-wide Association Study. *Genomics Proteomics
Bioinformatics* **19**, 619-628, doi:10.1016/j.gpb.2020.10.007 (2021).

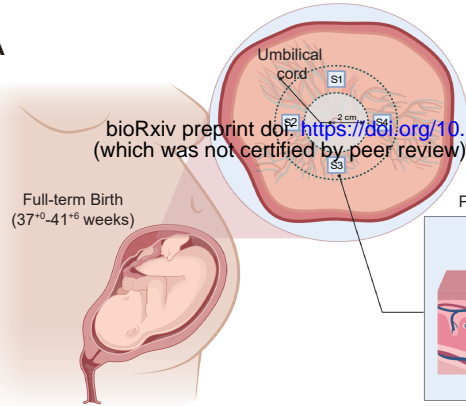
979 77 Choi, S. W. & O'Reilly, P. F. PRSice-2: Polygenic Risk Score software for biobank-scale
980 data. *Gigascience* **8**, doi:10.1093/gigascience/giz082 (2019).

981 78 Boughton, A. P. *et al.* LocusZoom.js: Interactive and embeddable visualization of
982 genetic association study results. *Bioinformatics*,
983 doi:10.1093/bioinformatics/btab186 (2021).

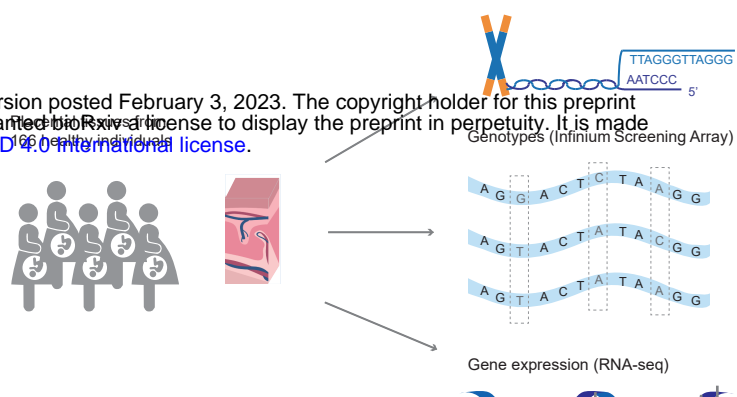
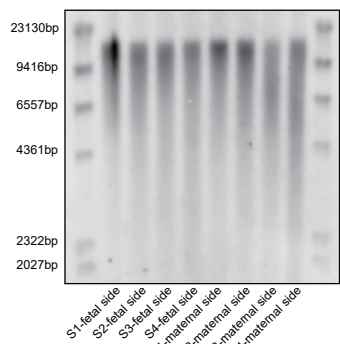
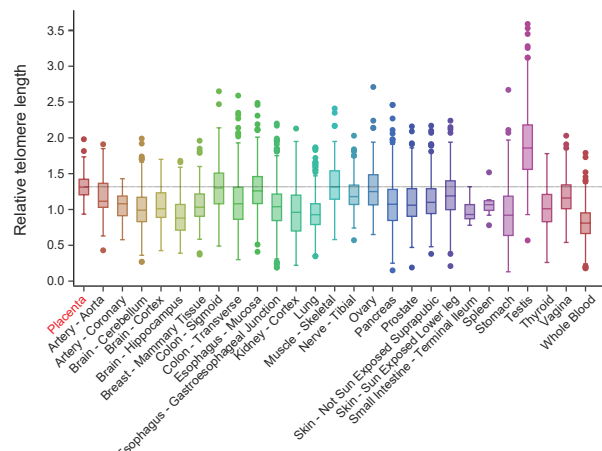
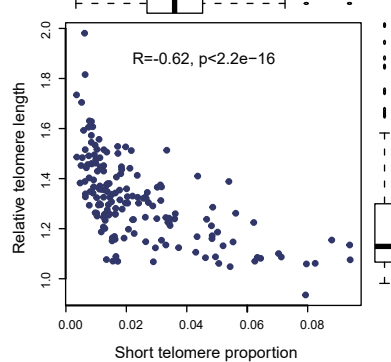
984 79 Genomes Project, C. *et al.* A global reference for human genetic variation. *Nature*
985 **526**, 68-74, doi:10.1038/nature15393 (2015).

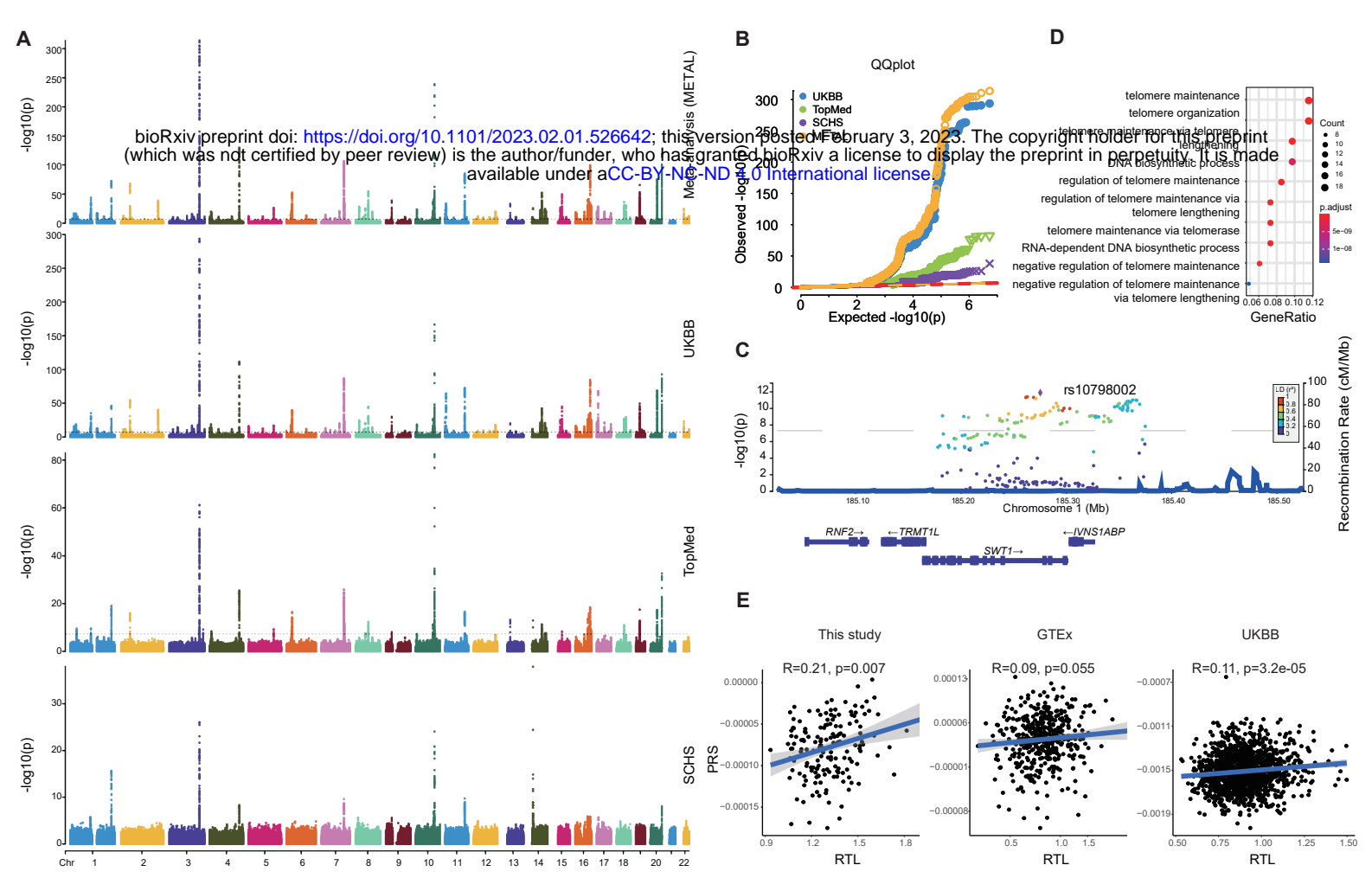
986 80 Friedman, J., Hastie, T. & Tibshirani, R. Regularization Paths for Generalized Linear
987 Models via Coordinate Descent. *J Stat Softw* **33**, 1-22 (2010).

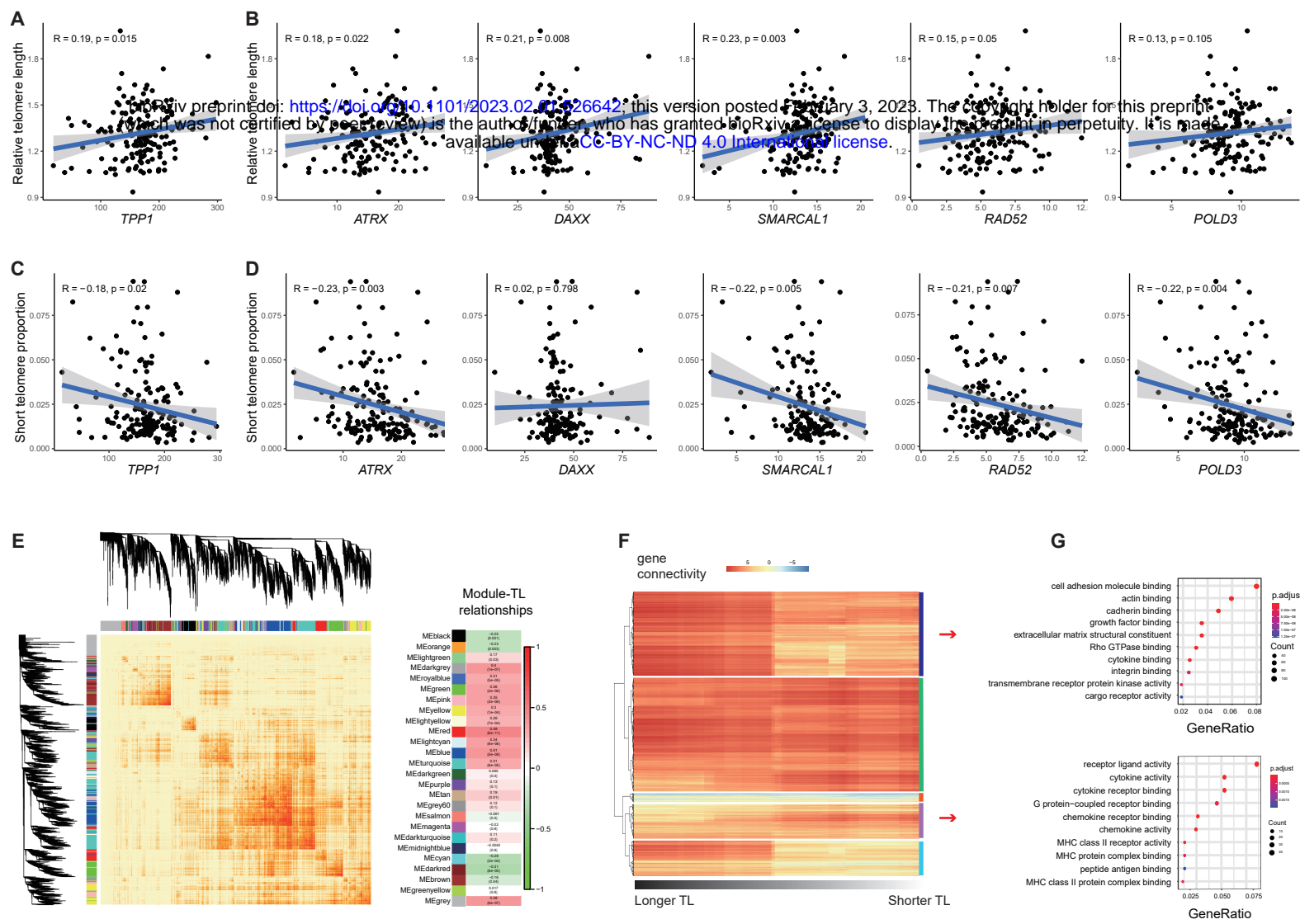
988
989

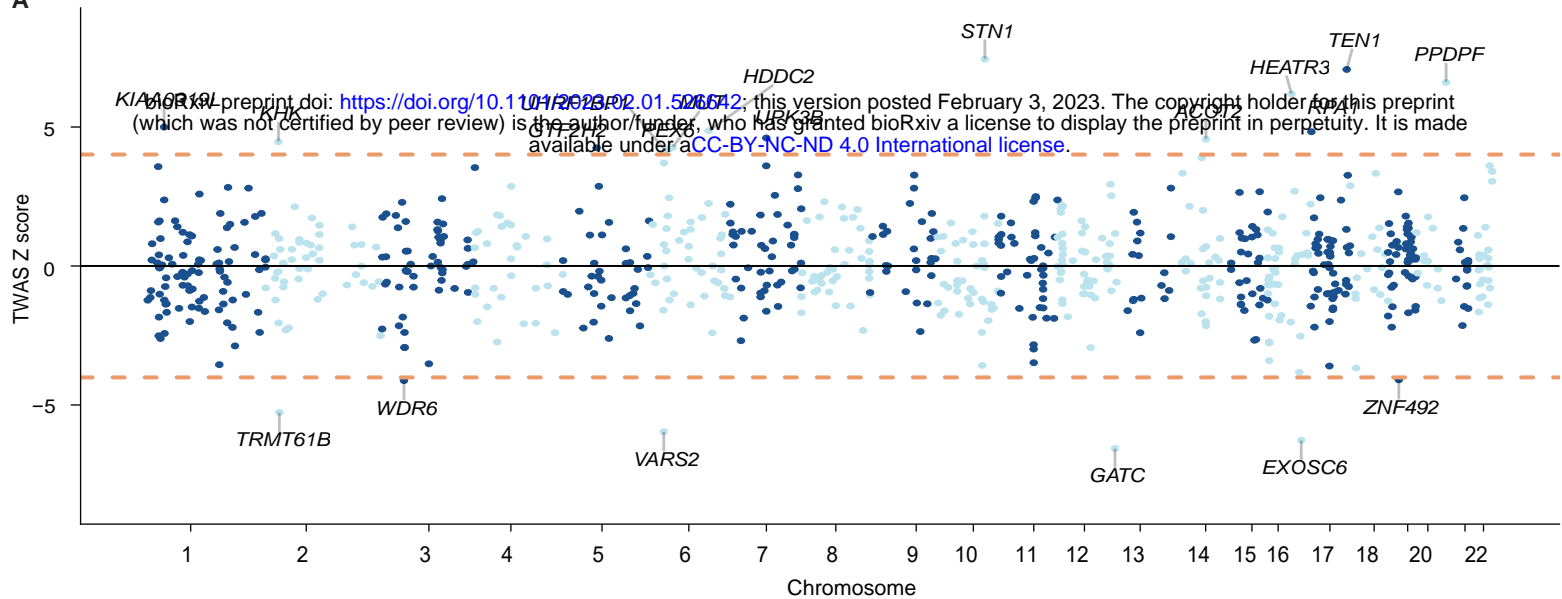
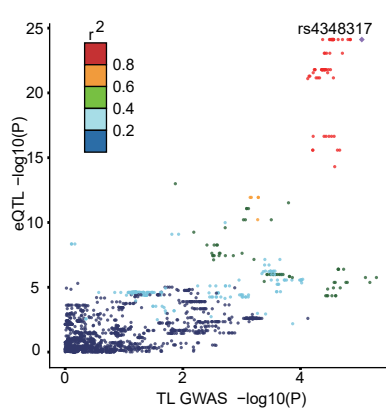
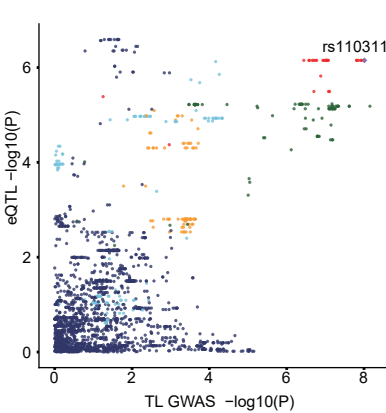
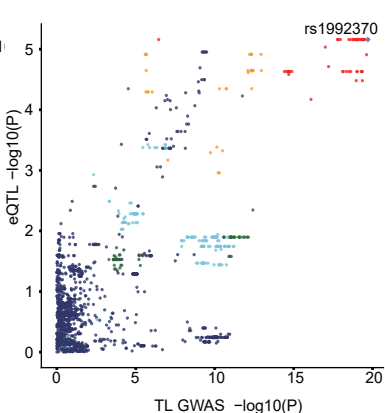
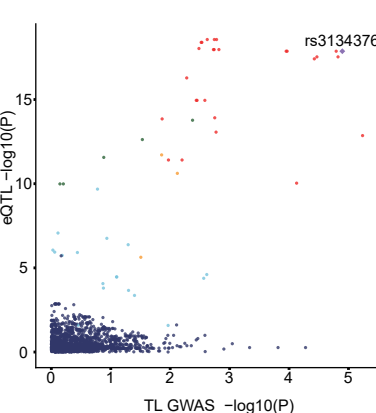
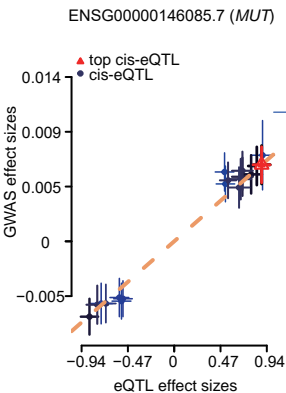
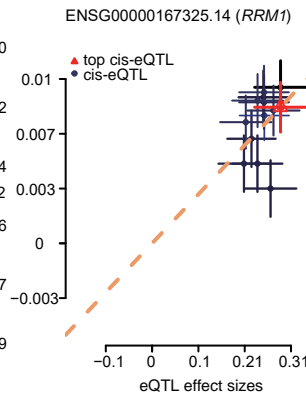
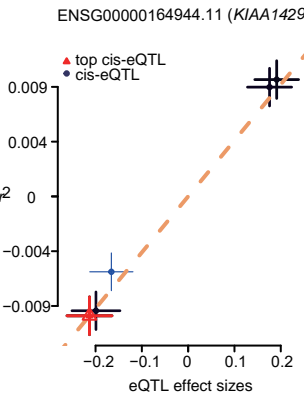
AFull-term Birth
(37⁰-41⁶ weeks)

bioRxiv preprint doi: <https://doi.org/10.1101/2023.02.01.526642>; this version posted February 3, 2023. The copyright holder for this preprint (which was not certified by peer review) is the author/funder, who has granted bioRxiv a license to display the preprint in perpetuity. It is made available under aCC-BY-NC-ND 4.0 International license.

B**C****D****E**





A**B****C****D****E****F****G****H****I**